GEOPHYSICS, VOL. 59, NO. 9 (SEPTEMBER 1994); P. 1392–1404, 15 FIGS., 1 TABLE.

An integrated target-oriented prestack elastic waveform inversion: Sensitivity, calibration, and application

Gee Shang Pan*, Chi. Y. Young*, and John P. Castagna‡

ABSTRACT

An integrated target-oriented prestack elastic waveform inversion procedure is implemented to estimate lithology, fluid type, and pay thickness of a layered target zone from surface seismic *PP* reflection data. The integrated inversion procedure consists of three parts: data processing and preparation, iterative seismic inversion, and rock property integration. In the data processing and preparation, the seismic field gathers are processed and transformed into plane-wave seismograms, and the well-logs are prepared for establishing a well tie. The well tie is established using synthetics from a layered model obtained from blocking sonic, shear sonic, and density logs. The layered model is later used as the a priori starting model for the iterative seismic inversion. Based on the a priori starting model and using the processed plane-wave seismograms as input, *P*-wave velocity (V_P), *S*-wave velocity (V_S), density (ρ), and thickness (h) of each layer in the layered target zone are estimated at each CDP location in the iterative seismic inversion. Through the rock property integration, the inverted seismic parameters are related to the reservoir properties: the lithology/fluid contents, and the net pay thickness.

Synthetic examples of gas-related bright spot models are used to illustrate the functionality of the procedure. The sensitivity and the vertical resolution of the inversion procedure are investigated. Under favorable conditions, the inversion procedure is able to estimate the net pay thickness down to a tenth of a wavelength. In noisy situations, the inversion tends to break down where the thickness of target is approximately equal to the tuning thickness.

The procedure was successfully applied to a gas-related shallow bright spot prospect offshore Gulf of Mexico. The lithology (sand shale distribution), V_P/V_S ratio, and the net pay thickness of gas-sand were derived for the prospect. The estimated net pay thickness of gas-sand was within acceptable error range when compared with the actual net pay thickness measured from well logs.

INTRODUCTION

Inversion of surface seismic data for reservoir properties, such as lithology type, fluid contents, and pay thickness is a very difficult problem. The solution of this problem involves solving two sets of inverse problems, and neither of them is trivial. The first one requires that the seismic (elastic) properties (such as *P*-wave velocity, *S*-wave velocity, and density . . .) be correctly derived from seismic data. The second requires the knowledge and understanding of local geological trends and rock physics properties so that the inverted seismic parameters can be related to the lithology, fluid contents, and ultimately the pay thickness. In this paper, using an integrated target-oriented approach, we demonstrate the feasibility of delineating gas-sand net pay thickness with seismic and well-log data from a shallow gas prospect offshore Gulf of Mexico.

The integrated inversion procedure consists of three parts: data processing and preparation, iterative seismic inversion, and rock property integration. In the data processing and preparation, the seismic field gathers are processed and transformed into plane wave seismograms, and the well-logs are prepared for establishing a well tie. The well tie is established using synthetics from a layered model obtained from blocking sonic, shear sonic, and density logs. The layered model is later used as the a priori starting model for the iterative seismic inversion. In the iterative seismic inversion, based on the a priori starting model and using the processed plane wave seismograms as input, *P*-wave veloc-

Manuscript received by the Editor March 3, 1993; revised manuscript received December 14, 1993.
*ARCO, 2300 W. Plano Parkway, Plano, TX 75075.
‡15375 Memorial Drive, Houston, TX 77079.

ity (V_P), S-wave velocity (V_S), density (ρ), and thickness (h) of each layer in the layered target zone are estimated at each common depth-point (CDP) location.

The iterative seismic inversion is the center of the integrated inversion procedure, and it is also the most computation-intensive part of the procedure. Recent advances in direct seismic waveform inversion in the plane-wave domain (Carrion et al., 1984; Pan et al., 1988; Pan and Phinney, 1989) and the concept of isolating target events from the overburden effects (Pan et al., 1990; Landrø et al., 1992; de Haas, 1992), make seismic prestack elastic waveform inversion practical for real data application. Seismic inversion can be posed as a problem of obtaining an earth model for which the synthetic seismograms best fit the observed data. The earth model can be derived using one of many different inversion schemes. In this paper, we adopted a linearized, iterative, elastic waveform inversion formalism (Tarantola and Valette, 1982; Tarantola, 1984) to solve the problem. We also chose a target-oriented approach to reduce the size of the problem and computation time. Subsequent to the iterative inversion, the inverted seismic/elastic properties are related to lithology and fluid type using petrophysical trend curves (Castagna et al., 1993), and in the case of a gas-sand reservoir, the net pay thickness of gas is estimated using information from a priori velocities, V_P versus V_S trends, Gassmann fluid substitution, and Wyllie's time-average equation (Castagna, 1993).

A series of synthetic seismograms are used to illustrate and calibrate the inversion procedure. First, the sensitivity of the inversion is discussed. Then, the vertical resolution of the procedure is demonstrated using noise-free data where the source wavelet, the amplitude scale factor, and the attenuation are known. Following that, the applicability and limitations of the procedure under noisy conditions are explored.

Finally, the procedure is tested on three prestack seismic lines that cover a shallow gas prospect offshore Gulf of Mexico. The net pay thickness of gas-sand is estimated for each seismic line and compared to the thickness measured from well logs to assess the predictability of the procedure.

INVERSION PROCEDURE

The integrated inversion procedure, as outlined in Figure 1, can be divided into three major components: data processing and preparation, iterative seismic inversion, and rock property integration. Each component is discussed in the sections that follow.

Data processing and preparation

Data processing and preparation is the most human labor intensive portion of our seismic inversion procedure. The main objective is to remove the noise effects from the well logs and seismic data so that the information provided by these two independent measurements can be related to each other.

Basically, there are two types of data processing and preparation prior to the iterative seismic inversion: seismic data processing and well-log preparation. The former subjects the seismic field gathers (PP signals) to a series of processing steps, which will be discussed in detail later in the results from real data section, to eliminate noise and then transforms the data (x, t) into the plane-wave (p, τ) seismograms. The latter involves editing and blocking of sonic, shear sonic, and density logs to the form that is suitable for generating a synthetic gather to establish the well tie. In the depth range (<2000 m) and frequency range (35 Hz dominant frequency) we are dealing with in this study, the number of layers blocked for the overburden portion of the model is in the range of 200 to 1000 layers and in the range of a couple of tens of layers for the target zone (Backus, 1962). If the shear sonic log is not available, it is derived using the method described by Greenberg and Castagna (1992). To what extent the well logs and seismic data need to be, and can be, processed to establish a high quality well tie remains a research issue. It often requires an iterative approach to accomplish the task. However, the importance of a high quality well tie can never be overstressed because it provides the time-depth relation and the petrophysical link between the seismic data and the a priori starting model for the iterative seismic inversion, as well as the amplitude scale factor between the observed and synthetic seismic data. During the process of establishing the well tie, a wavelet is also extracted by the method described by Nyman et al. (1987). The wavelet will be used for inversions at all the CDPs of the same seismic line. After an overburden correction is applied to the transformed seismic data, a time window is then selected that includes the target reflection

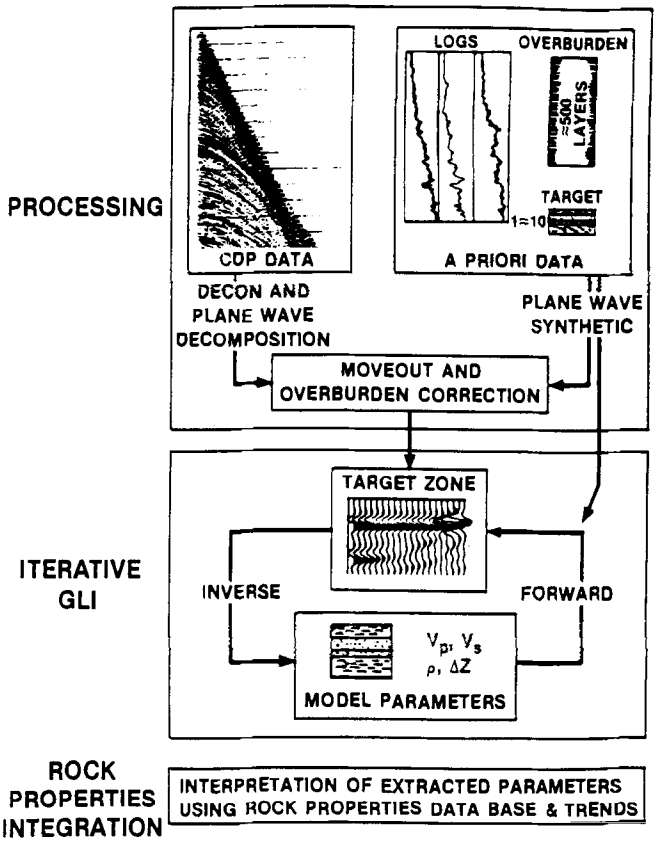

FIG. 1. The schematic representation of the integrated inversion procedure. It consists of three parts: data processing and preparation, iterative seismic inversion, and the rock property integration.

event for seismic inversion. For areas with multiple gas zones or complex structures above the target, sophisticated overburden corrections such as the approaches proposed by Gassaway (1984) and Cox and Wapenaar (1992) are popular. The specific overburden correction used in this paper is layer-stripping of the overburden effects by an equivalent composite layer.

Iterative seismic inversion

Using the time-windowed prestack seismic data in the intercept time and ray parameter (τ, p) domain and the a priori starting model as input, V_P (P-wave velocity), V_S (S-wave velocity), ρ (density), and h (layer thickness) of each layer in the layered target zone at each CDP location are estimated in the iterative seismic inversion.

Following Tarantola (1984) and Tarantola and Valette (1982), the following expressions are implemented in the iterative inversion:

Minimize

$$s(\mathbf{m}_k) = [\mathbf{d} - f(\mathbf{m}_k)]^T \mathbf{C}_d^{-1} [\mathbf{d} - f(\mathbf{m}_k)] + [\mathbf{m}_k - \mathbf{m}_o]^T \mathbf{C}_m^{-1} [\mathbf{m}_k - \mathbf{m}_o], \quad (1)$$

where,

$$\mathbf{m}_{k+1} = \mathbf{m}_k + \mathbf{W}\{\mathbf{C}_m \mathbf{G}_k^T \mathbf{C}_d^{-1} [\mathbf{d}_o - \mathbf{m}_k] - (\mathbf{m}_k - \mathbf{m}_o)\}, \quad (2)$$

$$\mathbf{W} = (\mathbf{I} + \mathbf{C}_m \mathbf{G}_k^T \mathbf{C}_d^{-1} \mathbf{G}_k)^{-1}, \quad (3)$$

where s is the objective functional, $\mathbf{G} = \partial f / \partial \mathbf{m}$ is the Fréchet derivative, $\mathbf{d}$ is the observed data, $f(\mathbf{m}_k)$ is the synthetic seismograms computed from the model $\mathbf{m}$ of the kth iteration, $\mathbf{m}_o$ is the a priori starting model, $\mathbf{C}_d$ is the a priori data covariance, $\mathbf{C}_m$ is the a priori model covariance, -1 is the inverse, and T is the transpose. The computed waveforms in the p, τ domain for each candidate model are compared with the p, τ transformed observed traces. The model perturbation, $\mathbf{W}\{\mathbf{C}_m \mathbf{G}_k^T \mathbf{C}_d^{-1} [\mathbf{d} - \mathbf{m}_k] - (\mathbf{m}_k - \mathbf{m}_o)\}$, is applied to the candidate model at each iteration. This process goes on until the inversion satisfies the prescribed convergence criteria. Three convergence criteria are used in the process: when the power of the residual seismograms is less than 20 dB of that of the input seismograms, when the maximum number of iteration is reached (15 iterations), and when the model perturbation is small compared with the previous iteration (<0.5%).

The p, τ domain formulation of the problem has computational advantages over the conventional approach in the space and time domain (Pan et al., 1988). For the forward problem, we use Kennett's (1983) reflectivity method to generate the synthetic waveforms in the p, τ domain directly. The Fréchet derivative and the Hessian which relates data residual to model perturbation are computed using finite differences. A staging strategy through iteration, starting with a small p range and then slowly increasing the range, is used to stabilize the inversion. A similar approach, starting with a narrow low-frequency band and then slowly widening the bandwidth, is also recommended.

It is a well-known fact that seismic inversion is intrinsically nonunique. This problem can be alleviated by incorporating a priori information (regularization) into the inversion procedure. A priori information can be as broad as intelligent guesses and regional geological information, or as detailed and specific as well-log information. In principle, well controls and their statistical properties can be used to derive the a priori starting model $\mathbf{m}_o$ and a priori model covariance $\mathbf{C}_m$. The properties and statistics derived from well control also provide important trend information for the rock property integration.

The incorporation of model and data covariances in the inversion scheme equation (1) amounts to the introduction of a generalized damping factor. The philosophy is similar to that of Levenberg (1944) and Marquardt (1963) in that the solution at each linearized iteration lies between solutions of the steepest descent and the least-squares methods to ensure a stable and rapid convergent solution. Assuming that the errors of the seismic traces are uncorrelated, Tarantola (1984) suggested that the data and model covariance operators be:

$$\mathbf{C}_d(\mathbf{r}_g, t; \mathbf{r}_s | \mathbf{r}'_g, t; \mathbf{r}'_s) = \sigma_{gs}^2 \delta_{gg'} \delta_{ss'}, \quad (4)$$

and

$$\mathbf{C}_m(\mathbf{r}, t; \mathbf{r}') = \frac{1}{(2\pi)^{1/2}} \frac{\sigma_m^2}{a} \exp\left[-\frac{1}{2} \frac{(\mathbf{r} - \mathbf{r}')^2}{a^2}\right], \quad (5)$$

where σ_{gs} is the error in the seismic trace for the gth receiver and the sth source, σ_m is the a priori variation in the model parameters, and a is the scale length over which the model is expected to be smooth. We further assume that the model parameters are not correlated, and the model covariance essentially reduces to a model variance. Where well controls are available in the prospect region, such as the one that will be discussed later in the real data case section, distributions of sonic, shear sonic, and density logs are generated to estimate the variation (variance) of P-wave velocity, S-wave velocity, and density according to different lithology type, depth interval, ... etc. The data variance is derived by analyzing the ambient noise in the seismic section before first breaks. To what extent the choice of the damping factor is optimal can be verified by the conventional trade-off curve (Backus and Gilbert, 1970) between the error of data and spread of model (Jordan and Franklin, 1971; Yomogida and Aki, 1987). It is possible but time consuming to determine the proper data variance and model variance for each parameter in each layer, but constant model and data variances are chosen instead. Using normalized model perturbation ($\delta V_P/V_P$, $\delta V_S/V_S$, $\delta\rho/\rho$, and $\delta h/h$) and ft/s, g/cm^3, and ft as velocity, density, and layer thickness units, respectively, the damping factor used for the synthetic and real data cases is $10^{-3.5}$.

To further constrain our inversion procedure, the inverted parameters are hardbound by well-log–derived extremes. For the real data inversion that will be discussed later, the shale properties above and below the target zone are not perturbed in the inversion. This approach helps stabilize the inversion and preserve the low-frequency component of the model that is provided by the a priori starting model.

Rock property integration

The model parameters V_P (P-wave velocity), V_S (S-wave velocity), ρ (density), and h (layer thickness) obtained from iterative seismic inversion are integrated with rock property trend curves to determine the "calibrated" reservoir properties such as rock type, fluid type, and net pay thickness (Castagna et al., 1993). For the case of gas-sand delineation,

the inverted seismic P-wave impedance ($V_P * \rho$), and S-wave impedance ($V_S * \rho$) are plotted against the shale, brine-sand, and gas-sand trend curves to infer the sand-shale lithology distribution. The V_P/V_S ratio and Wyllie's time-average equation are used to determine the presence of gas and its net pay thickness. The net pay thickness can be estimated (but the distribution cannot be resolved) below tuning from the inverted V_P/V_S (or equivalently, Poisson's) ratio of an interval in which only a fraction is gas pay. Figure 2 shows a crossplot of inverted Poisson's ratios and P-wave impedances for the shallow gas prospect described in a later section. A priori, we expect gas-sands to have Poisson's ratios of about 0.1 and brine-sands and shales to have Poisson's ratios above 0.4 in this locality. To the contrary, a continuum of Poisson's ratios is observed because some intervals are not entirely gas pay and exhibit a composite Poisson's ratio averaged in some way between gas-sand and brine-sand or shale. By assuming a time-average relationship for the layers for which the composite Poisson's ratio has been inverted, and using a priori velocities, V_P versus V_S trends, and Gassmann fluid substitution, the fractional gas-sand thickness within each composite layer can be computed (the net pay thickness is determined—not the distribution of pay sand). For the special case of a sand interval with almost equal V_S above and below the gas/water contact and known average velocities for the gas and water-saturated intervals, the fractional gas sand thickness X_{gas} can be extracted from the inverted V_P/V_S by (Castagna, 1993):

$$X_{gas} = \frac{1/V_P^{br} - (V_S/V_P)/V_S^{br}}{1/V_P^{br} - 1/V_P^{gas}}, \tag{6}$$

where, V_P^{br} is the brine-sand P-wave velocity, V_P^{gas} is the gas-sand P-wave velocity, and V_S^{br} is the brine-sand S-wave velocity.

As V_P/V_S is one of the more robust parameters obtainable from seismic inversion, the predicted X_{gas} is also robust, provided the above assumption is valid. It is a nontrivial task to estimate a single amplitude scale factor for the target window between the observed traces and synthetic traces in the multi-offset domain. More often than not, the amplitude scale factor established at the well tie is not exact. Inevitably, the net pay thickness estimated from seismic data is biased by the inexactness of this amplitude scale factor. The amplitude scale factor is further improved by calibrating the net pay thickness obtained from seismic data at the well tie to that measured from the well logs. Thus, this method is most applicable to extrapolation from existing well control. Assuming that the energy between CDPs is properly balanced by careful data acquisition and processing, the amplitude scale factor obtained at the well control is subsequently applied to the pay thickness derived from all the other CDPs of the same seismic line. From our experience with real seismic data inversion, this scale factor is usually between 0.8 to 1.2.

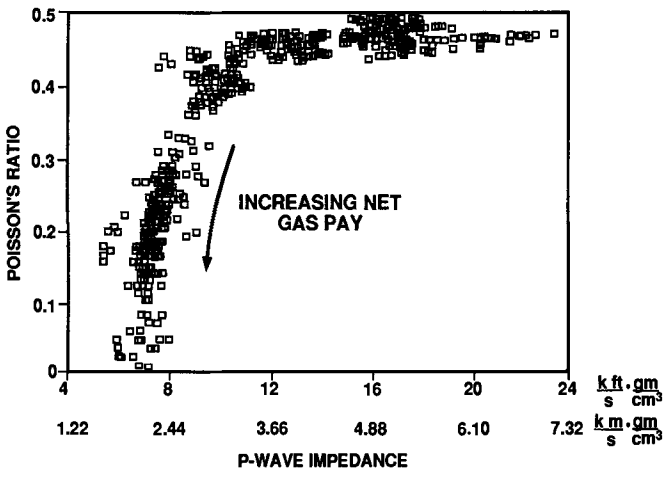

FIG. 2. Crossplot of the inverted Poisson's ratios and P-impedance for the gas prospect studied.

RESULTS FROM SYNTHETIC DATA

Model definition

A total of 11 models were created for synthetic study (Figure 3). Table 1 shows the model parameters for the different rock types used. All 11 models have the same lithological sequence, a 100-ft (30-m) thick sand layer embedded in shale with the top interface between shale and sand at a depth of 4200 ft (1300 m). The sand layer has two members. The top member is filled with gas and the bottom member with brine. Model 1 has no gas-sand member; it is a 100-ft (30-m)-thick brine-sand encased in shale. From models 2 to 11, the thickness of the gas-sand member progressively increases from 10 ft (3 m) to 100 ft (30 m) in increments of 10 ft (3 m). Therefore, model 11 has 100 ft (30 m) of gas-sand and no brine-sand.

For each of the 11 models, 17 synthetic traces were generated in the τ, p domain. The incident angle at the target reflector ranges from 3 to 40 degrees. All the synthetic data were moveout corrected using the constant velocity of shale; a 150 ms window was selected to include the target reflection event. This procedure is equivalent to a perfect overburden correction. These data sets are the "noise-free" data to test our inversion results.

Testing was carried out using noise-free, random noise, and coherent noise data. Random noise data were generated with the same frequency band as that used for the noise-free data sets, normalized, and superimposed on the noise-free data with a specific S/N ratio (measured in power). The coherent noise for each data set was created by applying a time shift to each trace in the noise-free seismic data. From trace 1 (near offset) to trace 17, the time shift increases from -16 ms to $+16$ ms with an increment of 2 ms between traces. The time-shifted data simulates a negative-slope event, such as a multiple, that crosses the original events at trace 9. This coherent noise represents one of several possible

Table 1. Model parameters for rock types.

lithology	V_P	V_S	ρ	Q_P	Q_S
Shale	2896	1448	2.25	300.	100.
Gas-sand	2280	1424	1.90	300.	100.
Brine-sand	2850	1425	2.13	300.	100.

Note: The unit for velocities V_P and V_S is m/s and that for ρ is gm/cm^3.

types of uncorrected noise from the data processing step. Each coherent noise data panel was scaled with a prescribed S/N ratio before being added to the corresponding noise-free data to generate the coherent noise data for testing.

In contrast to the data processing and preparation used for real data, in the synthetic study that follows the starting model and the wavelet are given. The starting model is specified as all shale to fully test the capability of our inversion algorithm. The model consists of three identical 35-ft (11-m) thick shale layers embedded between a 4200 ft (1300 m) thick shale overburden and a shale lower half-space. The wavelet is a 35-Hz Ricker wavelet for both the data synthetics and the inversion.

Sensitivity analysis

Given a data covariance, a model covariance, and a test model in equation (1), it is possible to compute the misfit (objective) functional to analyze the sensitivity of an inversion. The analysis can be done by systematically perturbing any of the model parameters over the admissible model space. For simplicity, we consider only the weighted data residual of equation (1), and only two model parameters are allowed to change in our sensitivity analysis. Using model 6 in Figure 3 as the true model, we have computed many misfit contour maps for different combinations of perturbation of the model parameters. Shown in Figure 4 is a typical misfit

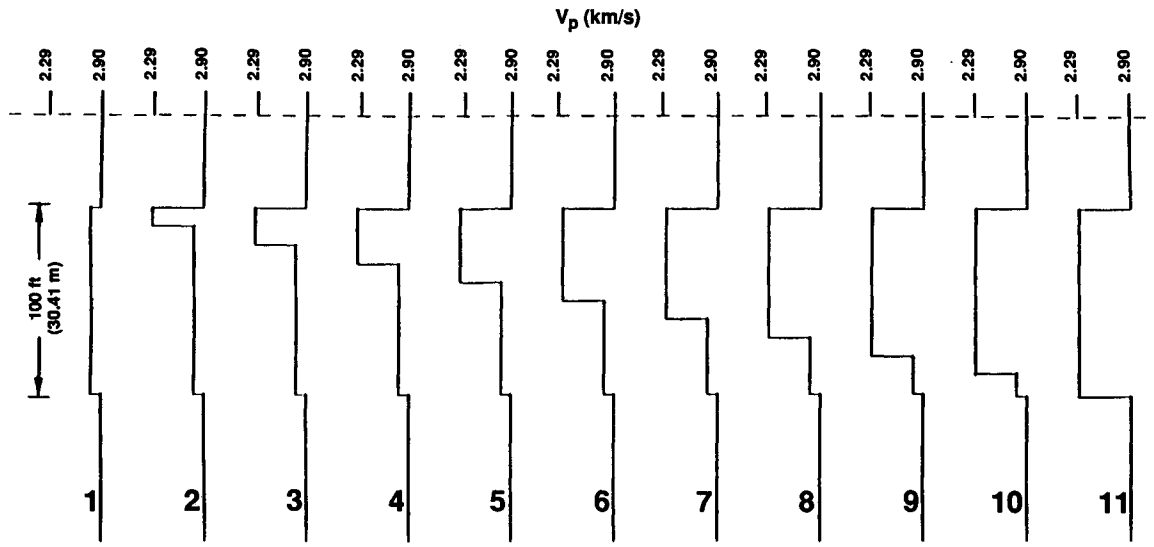

FIG. 3. The "true" model for inversion. The thickness of the gas-sand layer increases progressively from 0 to 100 ft (30 m) at 10-ft (3-m) increments.

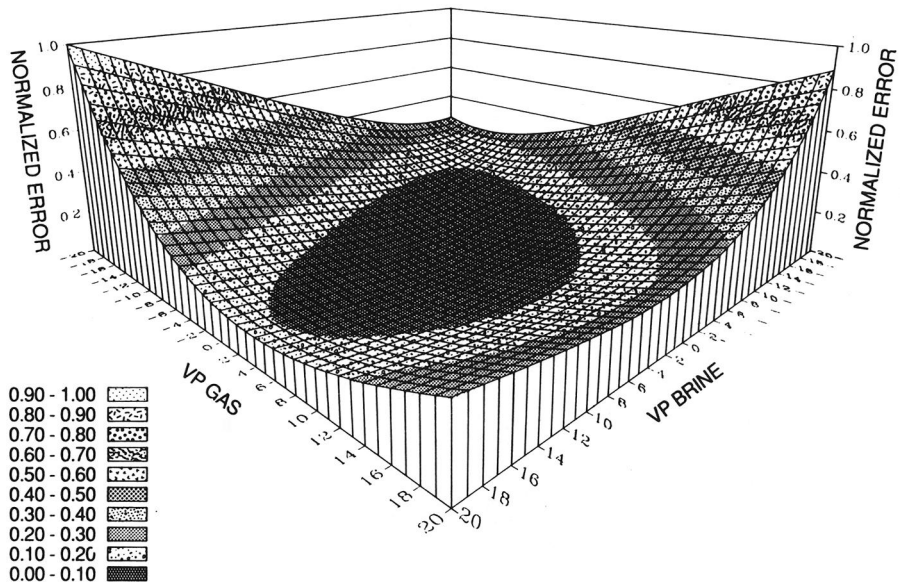

FIG. 4. The sensitivity analysis for V_P^{gas} versus V_P^{br} in the τ, p domain.

contour map computed over a ±20 percent perturbation of brine-sand P-wave velocity (V_P^{br}) versus gas-sand P-wave velocity (V_P^{gas}). Every plot of this type requires 1681 (41 × 41) realizations of the forward computation. The main conclusions of this study can be summarized as:

1) The misfit surface is skewed implying that there is always a trade-off between any two parameters.
2) Without noise and with a limited time window, this synthetic problem is fairly linear; that is, starting from any point on the misfit surface, an inversion should converge.
3) The misfit surface provides a clear illustration of the nonuniqueness problem of seismic inversion. Any model along the same contour line fits the observed data equally well in a least-squares sense. Given a specific misfit value, an inversion has multiple answers.
4) The misfit surface is very flat near the center which implies that many models in the central region will fit the data almost equally well. This is why a priori model constraints are important in that they help narrow the range of multiple answers.
5) For our target inversion, the sensitivity of the model parameters in terms of percentage perturbation decreases from V_P to ρ to V_S to h. Thickness is the least sensitive parameter (Figure 5).

Resolution and calibration

Assuming that the wavelet, attenuation profile, and amplitude scale factor are known, we have tested the inversion procedure against noise-free, random noise, and coherent noise data sets. Applying the integrated inversion procedure to these data sets, the V_P, V_S, ρ profiles versus h were derived, and subsequently the net pay thickness of each data set was estimated using equation (6). A compilation of the predicted net pay thickness of gas from different types of data sets is shown in Figure 6. For noise-free data, the vertical resolution of the net pay estimation is as good as 20 ft (6 m), which is about one-tenth of a wavelength. As a result of the amplitude and traveltime ambiguity as shown in Figure 7, the inversion is most unstable and tends to break down when the thickness of the target is at about the tuning thickness (Neidell and Poggiagliolmi, 1977; Merckel and Nath, 1977). The tuning thickness for a 35-Hz center frequency Ricker wavelet and a V_P of 7480 ft/s (2280 m/s) is approximately 50 ft (15 m), which is the target gas-sand thickness for model 6 in Figure 3. In the presence of random noise, the pay thickness estimation is consistent except when the data set is extremely noisy (S/N = 1) and the target thickness is approximately equal to the tuning thickness. For coherent noise cases, the inversion generally overestimated the pay thickness and gave the largest error when the thickness of the gas layer was approximately the tuning thickness. It is interesting to note that even though the layer thickness estimate is incorrect in the noisy cases, the inversion procedure correctly discriminates the models with gas (model 2–11) from the model without gas (model 1). Detailed analysis to compare each inverted seismic parameter with the true model in all the synthetic cases shows that there is a strong trade-off between velocity and density, and that the more robust inversion parameters are P-impedance, S-impedance and V_P/V_S.

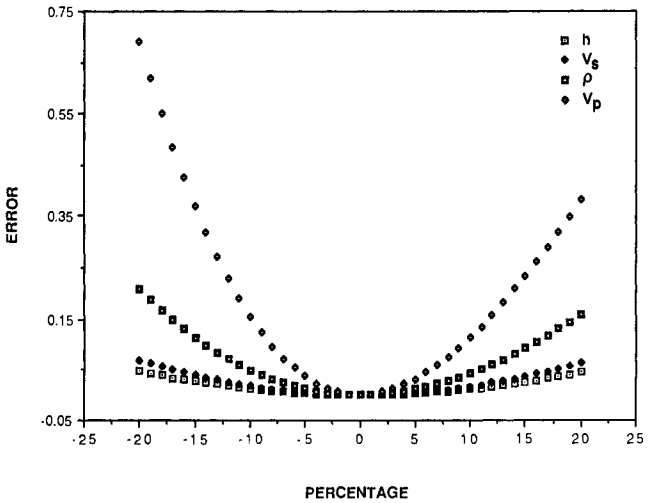

FIG. 5. The relative sensitivity between V_P, V_S, ρ, and h.

RESULTS FROM REAL DATA

The inversion procedure was applied to a gas prospect offshore Gulf of Mexico. Across this gas prospect, three seismic lines along with seven wells were used to test the procedure. Only one of the three seismic lines, line 1, will be discussed to illustrate the inversion results in detail. However, the net pay thickness derived at all of the seven well locations will be presented. Figure 8 shows seismic line 1 which has three well controls (well R, a dry well at CDP 973; well S, a gas well at CDP 1175; and well T, a gas well at CDP 1439). Both seismic lines 2 and 3 have two well controls. For all of the three seismic lines, the field seismic data, after channel recording gain quality control (QC) and correction, were sorted into common depth-point (CDP) gathers. After that, the following processing flow was applied to the CDP gathers: surface multiple removal, surface consistent wavelet deconvolution (Q compensation, signature deconvolution, autocorrelation averaged spiking deconvolution), velocity analysis, normal moveout (NMO) correction, S/N ratio enhancement (offset trace mixing, CDP mixing), reverse NMO, plane-wave decomposition through Radon transform, and overburden correction. The overburden-corrected plane-wave seismograms are the input data for iterative seismic inversion. Well S was used to derive the a priori starting model for inversion. A wavelet was extracted using the log-derived starting model and the seismic traces around the well for seismic line 1. Figure 9 shows the synthetic and AVO tie established for well S. Starting at the well, the iterative seismic inversion was performed for seismic line 1 in a CDP by CDP fashion. For seismic line 1, a 500 CDP line with ten layers in the target zone, it took about 10 CPU hours on Cray/XMP to complete the iterative seismic inversion.

It is instructive to investigate the inversion results at the locations of wells R, S, and T (Figures 10, 11, 12). Crossplots of the inverted P-wave impedance and S-wave impedance of each layer in the target zone against the shale, brine-sand, and gas-sand trend curves clearly indicate the presence of gas-sand in wells S and T but not in well R. The comparison

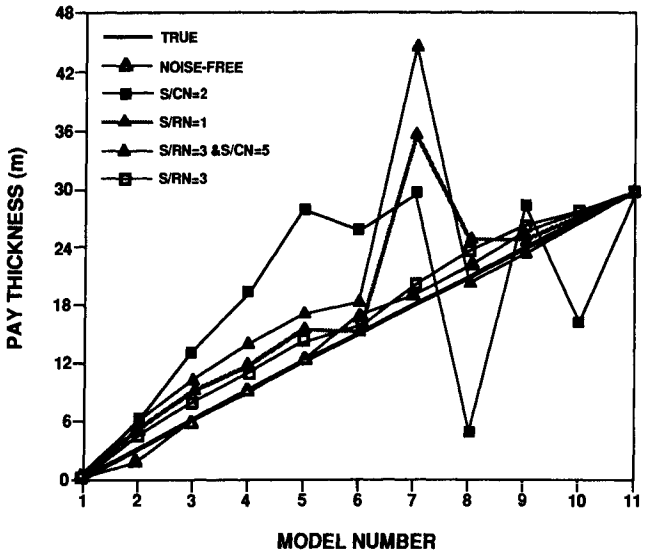

FIG. 6. The net pay thickness of gas from noise-free, random noise, and coherent noise data sets. S denotes signal, CN denotes coherent noise, and RN denotes random noise. Therefore, for example, $S/CN = 2$ means the signal to coherent noise ratio (in power) equals to 2. The pay thickness estimated from noise-free data gives a correct value down to 20 feet (6 m). The calibrating well for the scale factor is assumed at model 11.

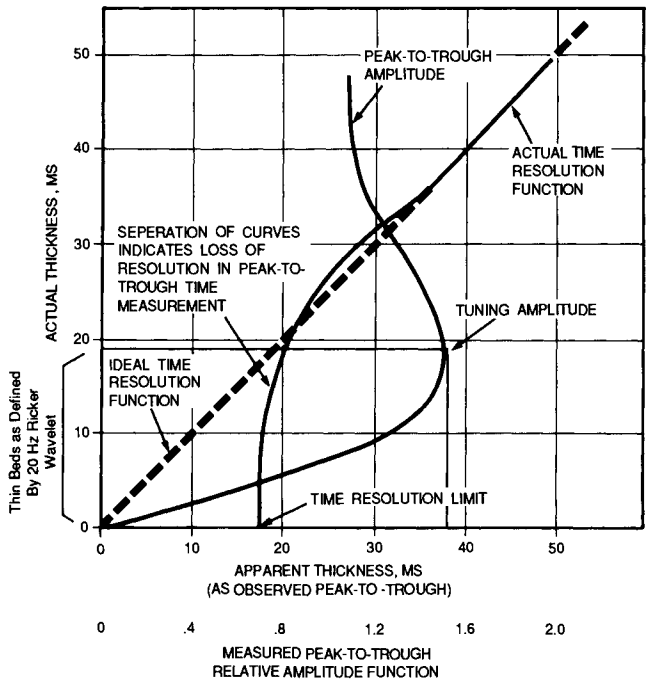

FIG. 7. The weak constraints of phase and amplitude information around tuning thickness (after Neidell and Poggiagliolmi, 1977). Around the tuning thickness, the peak-to-trough time approaches an asymptotic value and provides little resolution. In the same region, the amplitude information is also ambiguous, i.e., different thicknesses give the same amplitude.

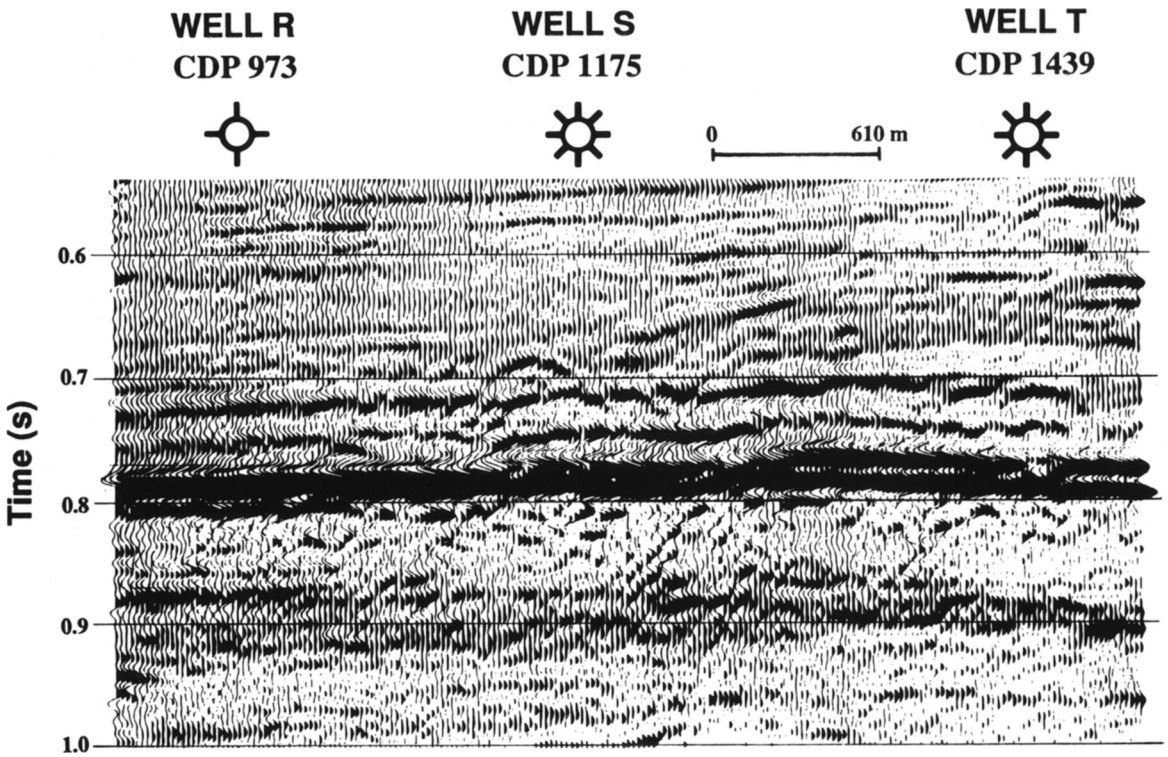

FIG. 8. The migrated stack seismic section of the line used to test the inversion procedure. The gas-related bright spot, the target event of our inversion procedure, is clearly seen at about 0.780 s.

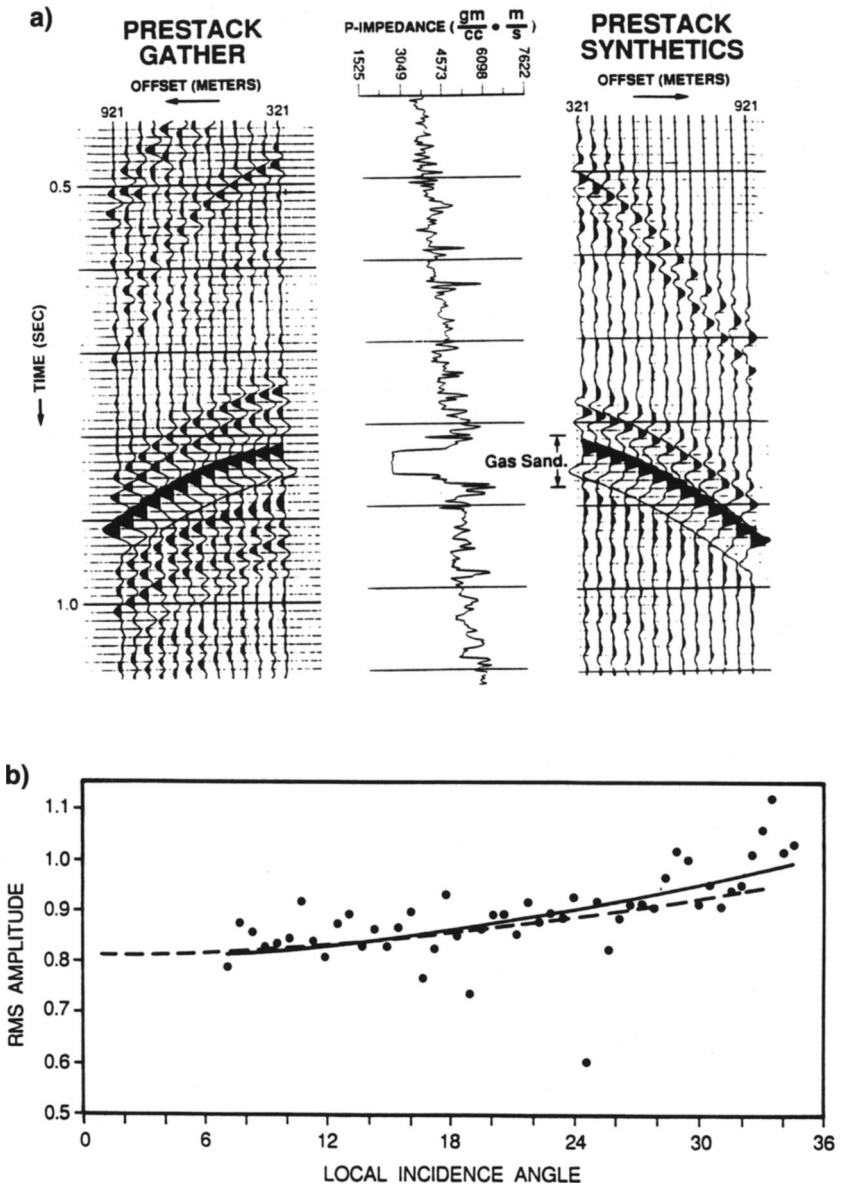

FIG. 9. The synthetic (a) and the AVO (b) tie of well S. The dashed line is the theoretical Zoeppritz response and the solid line is the least-squares fit of the observed responses (in dots).

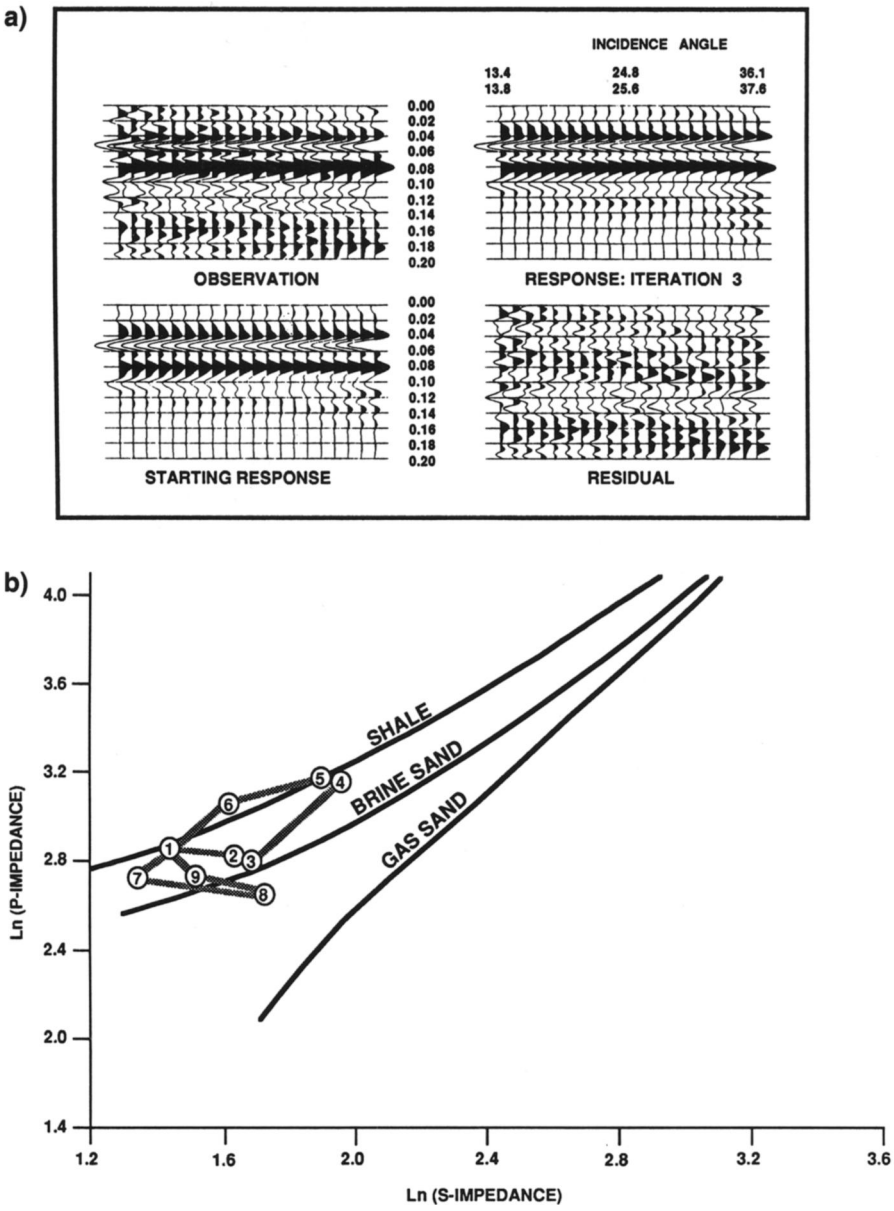

FIG. 10. The inversion results at CDP 973 around well R (a dry well). (a) The upper left hand panel is the transformed and (NMO)/overburden corrected observed data. The lower left-hand panel is the synthetic traces of the a priori starting model. The lower right-hand panel is the residual traces between the observed and the final synthetic seismograms, i.e., (b) the difference between the upper left-hand and the upper right-hand panels. The inverted seismic parameters, the *P*-wave impedance and the *S*-wave impedance of each layer determines a point on this log-log scale plot. The shale, brine-sand, and gas-sand trend curves are plotted for lithology determination. The location (denoted by the circled numbers) of each layer's *P*-wave and *S*-wave impedances is used to infer the sand-shale percentage by linearly interpolating between the shale and sand trends.

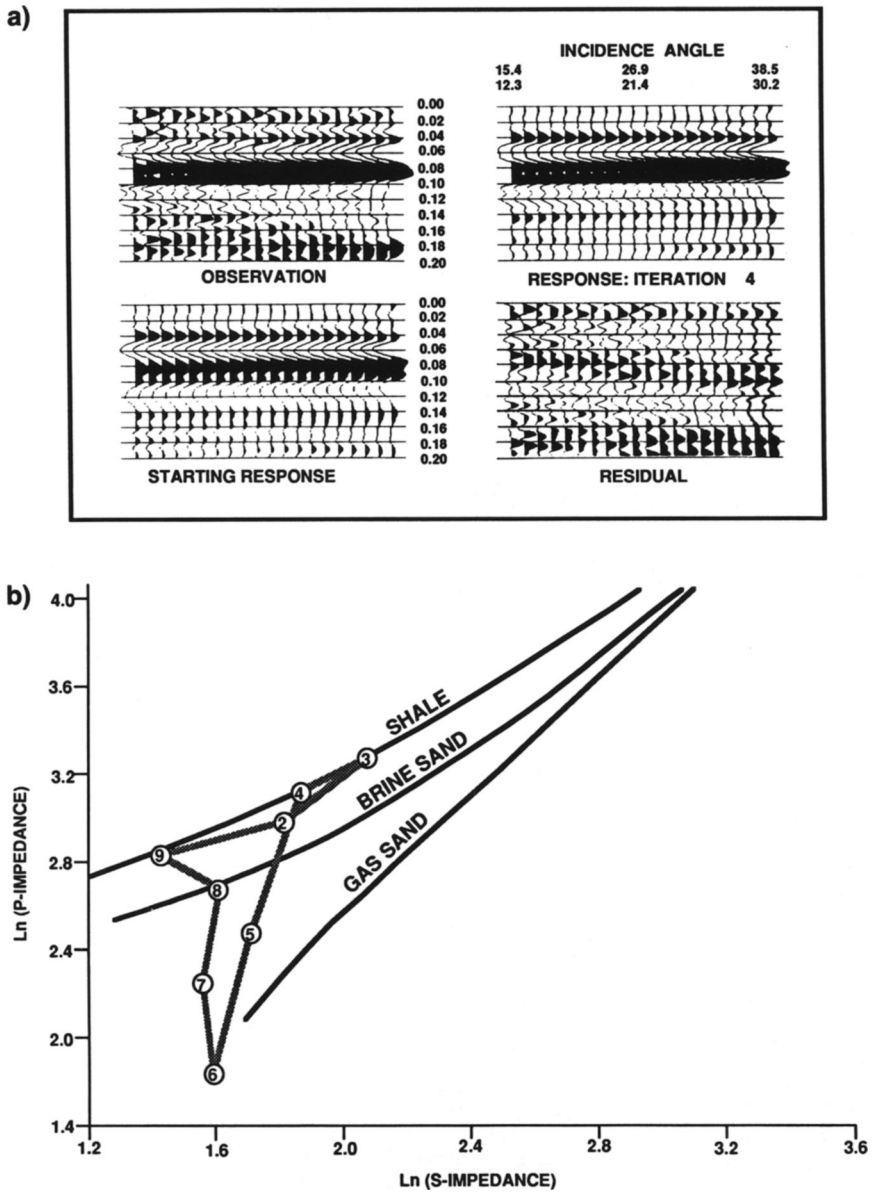

FIG. 11. The inversion results at CDP 1175 around well S (a gas well). The layout and notations are the same as Figure 10.

of the V_P/V_S ratio, which is a well-known gas indicator, at the three locations is shown in Figure 13. The two gas wells clearly have very low V_P/V_S intervals, while the dry well has a higher V_P/V_S ratio. The P-impedance profile, V_P/V_S ratio profile, and the net pay thickness of gas along seismic line 1 are shown in Figure 14. The same procedure was repeated for seismic lines 2 and 3. Figure 15 shows a crossplot of observed versus predicted gas net pay thickness at the seven wells in this study. The two wells, one for seismic lines 1 and 2 and another for seismic line 3, which show perfect prediction are the calibration wells. The two points with no sand present are localized "shale-outs" (verified by side-tracking) that are a result of tidal channel cut into the pay sand. These local channel cuts are believed to be smaller than a Fresnel zone. Applying prestack migration after velocity analysis and before NMO correction may help reveal "gaps" in the pay zone and improve the accuracy of pay thickness prediction.

CONCLUSIONS

An integrated target-oriented prestack elastic waveform inversion procedure has been implemented. With noise-free data and under favorable conditions, it correctly estimates net pay thickness to as thin as one-tenth of a wavelength.

The nonuniqueness problem is observed in a synthetic study and is dealt with in the real data cases by incorporating a priori information into the inversion. Measured in percentage perturbation, P-wave velocity is the most sensitive

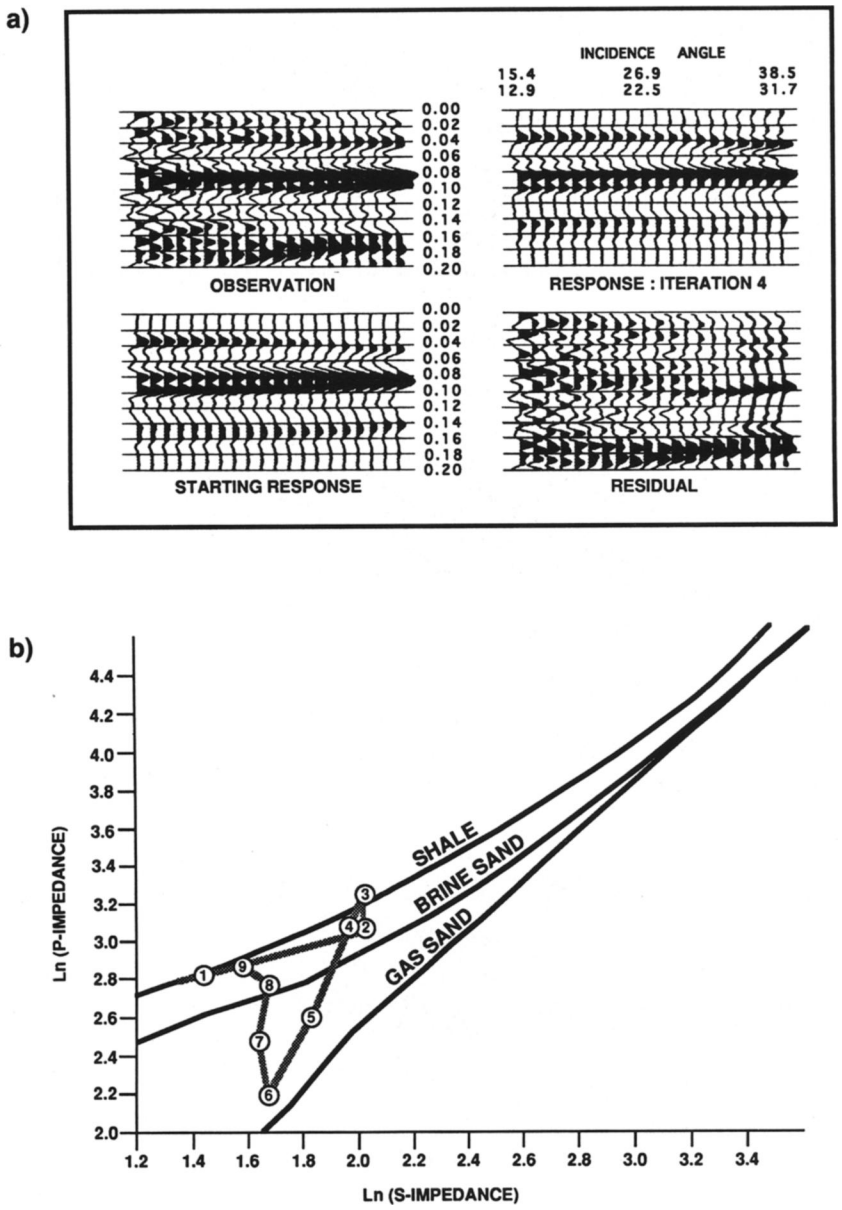

FIG. 12. The inversion results at CDP 1399 around well T (a gas well). The layout and notations are the same as Figure 10.

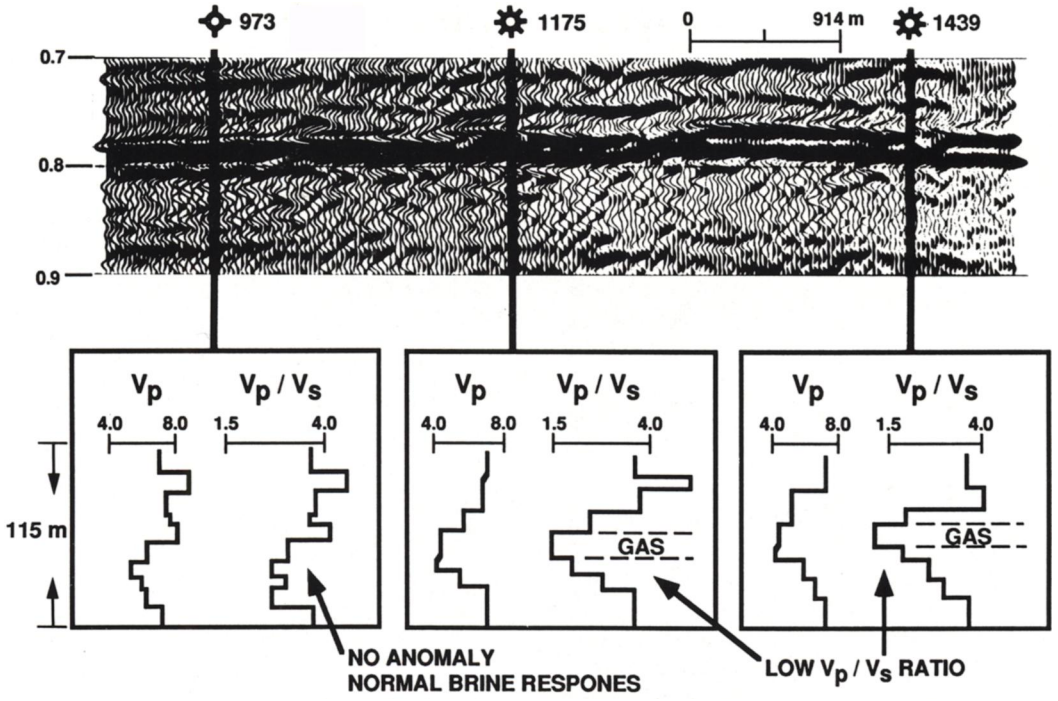

FIG. 13. Comparison of the inverted V_P and V_P/V_S ratio from CDP 973, 1175, and 1399. The low V_P/V_S zones are clearly correlated with the presence of gas intervals.

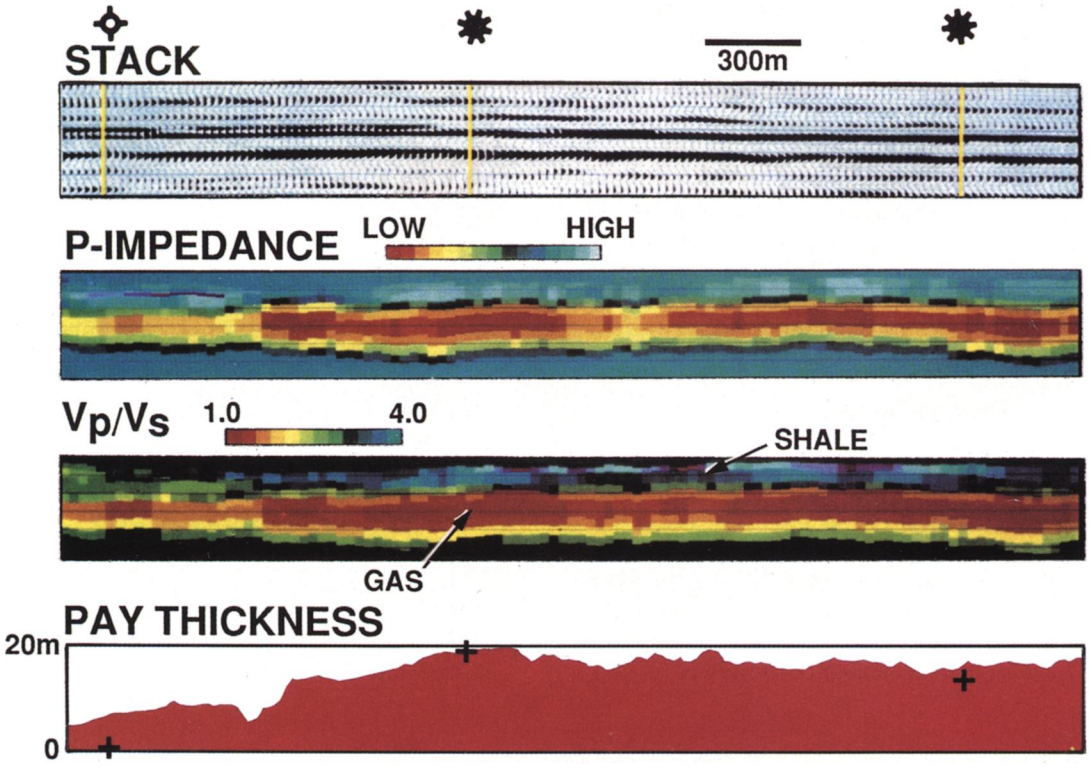

FIG. 14. The inverted P impedance profile, V_P/V_S profile, and the net pay thickness of gas-sand. The + denotes the pay thickness derived from well data.

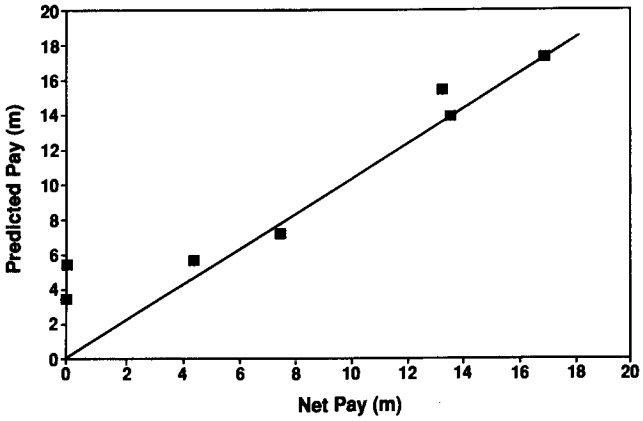

FIG. 15. A crossplot of the observed versus predicted gas thickness of all the seven wells used in this study.

parameter for a target waveform inversion and is followed in decreasing order by ρ, V_S, and h.

As expected, the L-2 norm least-squares inversion procedure is rather robust in dealing with random noise, but it has trouble handling coherent noise such as surface multiples and cross-cutting events because it is difficult for inversion algorithms to distinguish coherent noise from real signals. The best way to deal with coherent noise is to remove it in the data processing prior to inversion.

It is interesting to see that the inversion tends to break down around tuning thickness where both the phase and amplitude constraints are weak. In a different context and application, this situation was previously noticed by Neidell and Poggiagliolmi (1977) and Merckel and Nath (1977).

For practical applications, the procedure is most useful for delineating offshore, shallow, structurally simple, bright-spot events in the vicinity of well control where overburden effects and structural complications are minimal, and the statics are not severe. The inversion procedure was successfully applied to gas prospects offshore Gulf of Mexico. By attempting to fully utilize the information content of prestack seismic data as well as the petrophysical database and trend curves, we derived net pay gas-sand thickness with acceptable accuracy.

ACKNOWLEDGMENTS

We would like to thank the management of ARCO for allowing us to pursue and publish this paper. Special thanks to Al Garcia who developed the prototype inversion algorithm and set up the drafting tools. We would also like to thank Kabir Roy-Chowdhury and Charles Sicking for ARCO internal review of this manuscript. We appreciate the critical reviews and instructive comments by J. C. de Haas, D. E. Lumley, M. Landrø, and an anonymous reviewer.

REFERENCES

Backus, G., 1962, Long-wave elastic anisotropy produced by horizontal layering: J. Geophys. Res., **67**, 4427–4440.

Backus, G. and Gilbert, F., 1970, Uniqueness in the inversion of inaccurate gross earth data: Philosophical Trans. Roy. Soc. London A266, 247–276.

Carrion, Ph. M., Kuo, J. T., and Stoffa, P. L., 1984, Inversion method in the slant-stack domain using amplitudes of reflection arrivals: Geophys. Prosp., **32**, 375–391.

Castagna, J. P., 1993, AVO analysis—Tutorial and review, *in* Backus, M. and Castagna, J. P., Eds., Offset dependent reflectivity—Theory and practice: Investigation in Geophysics No. 8, Soc. Expl. Geophys., 3–36.

Castagna, J. P., Batzle, M. L., and Kan, T. K., 1993, Rock physics: The link between rock properties and amplitude-versus-offset response, *in* Backus, M. and Castagna, J. P., Eds., Offset dependent reflectivity—Theory and practice: Investigation in Geophysics No. 8, Soc. Expl. Geophys., 135–174.

Cox, H. L. H. and Wapenaar, C. P. A., 1992, Macro model estimation by common-offset migration or by shot record migration?: J. Seismic Expl., **1**, 29–38.

Gassaway, G. S., 1984, Effects of shallow reflectors on amplitude-versus-offset (seismic lithology) analysis: 54th Ann. Internat. Mtg., Soc. Expl. Geophys., Expanded Abstract, 665–669.

Greenberg, M. L. and Castagna, P. C., 1992, Shear-wave velocity estimation in porous rocks: Theoretical formulation, preliminary verification and applications: Geophys. Prosp., **40**, 195–210.

de Haas, J. C., 1992, Elastic stratigraphic inversion, an integrated approach: Ph.D. thesis, Delft University of Technology.

Jordan, T. H. and Franklin, J. N., 1971, Optimal solution to a linear inverse problem in Geophysics: Proc. National Academy of Science, **68**, 291–293.

Kennett, B. L. N., 1983, Seismic wave propagation in stratified media: Cambridge University Press.

Landrø, M., Helgesen, J., Chapel, F., and Picart, I., 1992, Target-oriented AVO inversion of North Sea data: 62nd Ann. Internat. Mtg., Soc. Expl. Geophys., Expanded Abstract, 870–873.

Levenberg, K., 1944, A method for the solution of certain nonlinear problems in least squares: Quarterly of Applied Mathematics, **2**, 164–168.

Marquardt, D. W., 1963, An algorithm for least-squares estimation of nonlinear parameters: J. Soc. Industrial and Applied Mathematics, **11**, 431–441.

Merckel, L. D. and Nath, A. K., 1977, Stratigraphic modeling and interpretation—Geophysical principles and techniques: *in* Payton, C. E., Ed., AAPG Memoir 26, 417–438.

Neidell, N. S. and Poggiagliolmi, E., 1977, Stratigraphic modeling and interpretation—Geophysical principles and techniques: *in* Payton, C. E., Ed., AAPG Memoir 26, 389–416.

Nyman, D. C., Parry, M. J., and Knight, R. D., 1987, Seismic wavelet estimation using well control: 57th Ann. Internat. Mtg., Soc. Expl. Geophys., Expanded Abstract, 211–213.

Pan, G. S. and Phinney, R. A., 1989, Full-waveform inversion of plane-wave seismograms in stratified acoustic media: Applicability and limitations: Geophysics, **54**, 368–380.

Pan, G. S., Phinney, R. A., and Odom, R. I., 1988, Full-waveform inversion of plane-wave seismograms in stratified acoustic media: Theory and feasibility: Geophysics, **53**, 21–31.

Pan, G. S., Young, C. Y., and Castagna, P. C., 1990, Sensitivity and resolution of a target-oriented prestack elastic inversion: 60th Ann. Internat. Mtg., Soc. Expl. Geophys., Expanded Abstract, 1173–1176.

Tarantola, A., 1984, Nonlinear inverse problem for a heterogeneous acoustic medium: Geophysics, **49**, 1259–1266.

Tarantola, A. and Valette, B., 1982, Generalized nonlinear inverse problem solved using the least-squares criterion: Rev. Geophys. Space Phys., **20**, 219–233.

Yomogida, K. and Aki, K., 1987, Amplitude and phase data inversions for phase velocity anomalies in the Pacific Ocean Basin: Geophys. J. Roy. Astr. Soc., **88**, 161–204.